The Intraflagellar Transport Protein IFT20 Recruits ATG16L1 to Early Endosomes to Promote Autophagosome Formation in T Cells

Francesca Finetti[1]*, Chiara Cassioli[1], Valentina Cianfanelli[2,3], Fabrizia Zevolini[1], Anna Onnis[1], Monica Gesualdo[1], Jlenia Brunetti[4], Francesco Cecconi[2,3,5] and Cosima T. Baldari[1]*

[1] Department of Life Sciences, University of Siena, Siena, Italy, [2] Cell Stress and Survival Unit, Center for Autophagy, Recycling and Disease (CARD), Danish Cancer Society Research Center, Copenhagen, Denmark, [3] Department of Pediatric Hemato-Oncology and Cell and Gene Therapy, IRCCS Bambino Gesù Children's Hospital, Rome, Italy, [4] Department of Medical Biotechnologies, University of Siena, Siena, Italy, [5] Department of Biology, University of Rome Tor Vergata, Rome, Italy

Lymphocyte homeostasis, activation and differentiation crucially rely on basal autophagy. The fine-tuning of this process depends on autophagy-related (ATG) proteins and their interaction with the trafficking machinery that orchestrates the membrane rearrangements leading to autophagosome biogenesis. The underlying mechanisms are as yet not fully understood. The intraflagellar transport (IFT) system, known for its role in cargo transport along the axonemal microtubules of the primary cilium, has emerged as a regulator of autophagy in ciliated cells. Growing evidence indicates that ciliogenesis proteins participate in cilia-independent processes, including autophagy, in the non-ciliated T cell. Here we investigate the mechanism by which IFT20, an integral component of the IFT system, regulates basal T cell autophagy. We show that IFT20 interacts with the core autophagy protein ATG16L1 and that its CC domain is essential for its pro-autophagic activity. We demonstrate that IFT20 is required for the association of ATG16L1 with the Golgi complex and early endosomes, both of which have been identified as membrane sources for phagophore elongation. This involves the ability of IFT20 to interact with proteins that are resident at these subcellular localizations, namely the golgin GMAP210 at the Golgi apparatus and Rab5 at early endosomes. GMAP210 depletion, while leading to a dispersion of ATG16L1 from the Golgi, did not affect basal autophagy. Conversely, IFT20 was found to recruit ATG16L1 to early endosomes tagged for autophagosome formation by the BECLIN 1/VPS34/Rab5 complex, which resulted in the local accumulation of LC3. Hence IFT20 participates in autophagosome biogenesis under basal conditions by regulating the localization of ATG16L1 at early endosomes to promote autophagosome biogenesis. These data identify IFT20 as a new regulator of an early step of basal autophagy in T cells.

Keywords: intraflagellar transport, vesicular trafficking, ATG16L1, early endosomes, autophagy, T cell

INTRODUCTION

Autophagy is a degradative process that subserves the dual function of eliminating damaged macromolecules and organelles while providing endogenous energy sources and building blocks to maintain cellular homeostasis (Dikic and Elazar, 2018). Similar to other cell types, T cells exploit autophagy as a quality control and pro-survival mechanism which is essential for the long-lasting maintenance of the naive peripheral T cell repertoire. The roles of autophagy are, however, not limited to T cell homeostasis. Autophagy participates in thymocyte development by sustaining the survival of double negative thymocytes and their transition to the double positive stage (Nedjic et al., 2008) and regulates both positive and negative selection via the MHCII loading pathway in thymic epithelial cells (Kasai et al., 2009). In the periphery, T cell activation and proliferation are fine-tuned by selective autophagy (Zaffagnini and Martens, 2016). In this context, the autophagy cargo is initially switched from mitochondria to macromolecules including inhibitors of T cell receptor (TCR) signaling (Hubbard et al., 2010; Valdor et al., 2014) and cell cycle (Jia et al., 2015). Subsequently, as T cells undergo differentiation, the autophagic degradation of the NF-κB regulator Bcl10 occurs (Paul et al., 2012). Autophagy also impacts on helper and cytotoxic T cell effectors, with Th1, Th2, and Treg cells relying on autophagy for survival (Kovacs et al., 2012; Kabat et al., 2016; Wei et al., 2016) and cytotoxic T lymphocytes (CTL) for their function and for memory maintenance (Puleston et al., 2014; Xu et al., 2014).

The autophagy machinery has been extensively characterized. Autophagy is initiated by the ULK complex, consisting of ULK1/2, ATG13, FIP200, and ATG101, which promotes phagophore nucleation through the class III PI3-K complex, consisting of VPS34, VPS15, BECLIN 1, and ATG14L. In order to engulf the cargo, the phagophore elongates and subsequently closes. These two steps involve the ATG12-ATG5 conjugation system, which is recruited to the phagophore by ATG16L. The conjugation system acts as an E3-like ligase to promote the cleavage and lipidation of ATG8/LC3, resulting in the phosphatidyl ethanolamine-conjugated form that binds to the phagophore membrane. Following phagophore closure, the resulting autophagosomes undergo dynein-dependent transport along the microtubules to a perinuclear location, where they fuse with lysosomes to become autolysosomes, delivering their cargo for degradation (Dikic and Elazar, 2018). This basic process is fine-tuned by a plethora of regulators and effectors. Among these is the intraflagellar transport (IFT) system, a multimolecular protein complex which controls the assembly of the primary cilium, a signaling organelle present in the majority of vertebrate cells (Pampliega et al., 2013; Prevo et al., 2017). Two integral components of the IFT system, IFT20 and IFT88, have been shown to mediate the transport of some components of the autophagic machinery to the cilium during cell starvation, with IFT20 binding ATG16L1 at the Golgi apparatus and shuttling it to the base of the cilium, wherefrom it enters the cilium with the assistance of IFT88 (Pampliega et al., 2013).

We have previously shown that, unexpectedly, IFT20 plays a key role in the activation of the non-ciliated T cells in a complex with other IFT components by regulating the assembly of the immune synapse, a specialized signaling interface that forms when a T cell encounters a cognate antigen presenting cell (Finetti et al., 2009, 2011). This function involves the ability of IFT20 to associate with the Golgi complex and endocytic compartments, the primary one among the latter being the early endosome, to control the intracellular traffic of the T cell antigen receptor and the transmembrane adaptor linker for activation of T cells (LAT) (Finetti et al., 2009, 2014; Vivar et al., 2016). Interestingly, we have recently implicated IFT20 in another vesicular trafficking-related process, the mannose-6-phosphate receptor-dependent transport of acid hydrolases to lysosomes, on which lysosome biogenesis and function depend (Finetti et al., 2020). Consistent with the central role of lysosomes in autophagy, both basal and starvation-induced autophagy are impaired in IFT20-deficient T cells (Finetti et al., 2020). However, the implication of the IFT system at early steps of autophagy in ciliated cells (Pampliega et al., 2013) suggests that IFT20 could participate in T cell autophagy also directly. Here, we show that IFT20 promotes ATG16L1 localization to the Golgi complex and early endosomes through its interaction with GMAP210 and Rab5, respectively. We demonstrate that under basal conditions IFT20 participates in autophagosome formation at early endosomes, but not at the Golgi apparatus, by allowing for the recruitment of ATG16L1 to early endosome-associated BECLIN 1 complex, thereby promoting local LC3-II accumulation. Our results identify IFT20 as an adaptor that targets ATG16L1 and downstream autophagy regulators to a specific endomembrane compartment, resulting in autophagosome biogenesis in T cells.

MATERIALS AND METHODS

Cells, Plasmids, and Transfections

Control, IFT20KD, and GMAPKD Jurkat T cell lines were generated as previously described (Finetti et al., 2009; Galgano et al., 2017). Jurkat T cells were stably transfected with the pEGFP-N1 plasmid construct encoding full-length IFT20, or a deletion mutant of IFT20 lacking aminoacid residues 73–132, which include the coiled-coil domain (ΔCC IFT20), or the respective empty vector. Stably transfected cells were selected in G418-containing medium at the final concentration of 1 μg/ml (Gibco/Thermo Fisher Scientific, MA, United States). Transient transfections were carried out by electroporation using pCMV-EGFP-C3-Rab5a (kindly provided by M. Zerial), pEGFP 2xFYVE (kindly provided by A. De Matteis), pEGFP-N1 IFT20-GFP, or pEGFP-N1 ΔCC IFT20-GFP [1 μg/1 × 10^6 cells in 800 μl of OPTI-MEM (Gibco/Thermo Fisher Scientific, MA, United States)] and analyzed 24 h post-transfection.

Cloning and Purification of Recombinant Proteins

GFP- and GST-tagged mutants of IFT20 were generated by cloning the sequences that encode the IFT20 N-terminus lacking the coiled-coil domain (ΔCC-IFT20, aa 1–73), the IFT20 C-terminus including the coiled-coil domain (CC-IFT20, aa 74–132), and the full-length protein (IFT20, aa 1–132) in-frame with the tags into the pEGFP-N1 (#6085-1 Addgene) and pGEX-6P-2

vectors (#27-4598-01 Addgene). The sequences were amplified by PCR using the primers listed in **Supplementary Table 1**. The 5'-ends of the primers were modified to add compatible restriction sites (*XhoI* and *KpnI* for pEGFP-N1, *EcoRI* and *XhoI* for pGEX-6P-2) and extra base pairs that ensure efficient DNA cleavage by restriction enzymes.

The recombinant GST fusion proteins were affinity purified on GSH-Sepharose (GE Healthcare, Italy) from bacterial cultures incubated with 0.25 mM isopropyl-β-D-thiogalactopyranoside (Sigma-Aldrich) overnight at RT and lysed in B-PER Complete Bacterial Protein Extraction Reagent (Thermo Fisher Scientific, MA, United States) according to the manufacturers' instructions.

Antibodies and Reagents

All primary commercial antibodies used in this manuscript are listed in **Supplementary Table 2**, where information about the dilutions used for immunoblotting and immunofluorescence is specified. Polyclonal anti-IFT20 antibodies (Pazour et al., 2002) were kindly provided by G. Pazour. Secondary peroxidase-labeled antibodies were from Amersham Biosciences. Alexa Fluor 488- and 555-labeled secondary Abs were from Thermo Fisher Scientific (anti-mouse 488, #A11001; anti-rabbit 488, #A11008; anti-mouse 555, #A21422; and anti-rabbit 555, #A21428). Chloroquine was purchased from Sigma-Aldrich (C6628).

Immunoprecipitation, *in vitro* Binding Assays and Immunoblotting

Immunoprecipitation experiments were performed as previously described (Finetti et al., 2020). Briefly, 5×10^7 cells/sample were lysed in 0.5% Triton X-100 in 20 mM Tris–HCl (pH 8), 150 mM NaCl in the presence of protease inhibitors (Sigma-Aldrich) and the phosphatase inhibitor sodium vanadate (Sigma-Aldrich). Postnuclear supernatants (2 mg/sample) were immunoprecipitated for 2 h at 4°C with gentle agitation using 2 µg of rabbit anti-IFT20 antibody (#13615-1-AP, Proteintech, United Kingdom), anti-ATG16L1 antibody (#8089S, Cell Signaling) or mouse anti-BECLIN 1 mAb (sc-48341, Santa Cruz), and protein A-Sepharose (PAS, 3 mg/sample, GE Healthcare, Italy), after a preclearing step on PAS (1 h, 3 mg/sample). Subsequently, all samples were washed 4X with 1 ml 0.5% Triton X-100 lysis buffer, resuspended in 15 µl Laemmli buffer (#B0007, Life Technologies/Thermo Fisher Scientific, MA, United States), boiled for 5 min and then subjected to SDS-PAGE.

In vitro-binding assays were carried out using recombinant GST, IFT20-GST, ΔCC IFT20-GST, or CC IFT20-GST on GSH-Sepharose precleared postnuclear supernatants from 5×10^7 cells/sample lysed in 0.5% Triton X-100 in the presence of protease and phosphatase inhibitors as described (Pacini et al., 1998). The binding reaction was performed for 2 h at 4°C with gentle agitation. Samples were washed 4X with 1 ml 0.5% Triton X-100 lysis buffer in the presence of protease and phosphatase inhibitors, resuspended in 15 µl Laemmli buffer, boiled for 5 min and subjected to SDS-PAGE.

Immunoblotting was carried out using peroxidase-labeled secondary antibodies and a chemiluminescence detection

kit (#34578, Thermo Fisher Scientific, MA, United States). Membranes were reprobed with control antibodies after stripping carried out using ReBlot Plus Mild Antibody Stripping Solution, 10× (#2502, Merck Millipore, Italy). Blots were scanned using a laser densitometer (Duoscan T2500; Agfa, Belgium) and quantified by using ImageJ 1.46r (National Institutes of Health, United States).

Immunofluorescence Microscopy and Colocalization Analyses

For immunofluorescence analysis, Jurkat cells were allowed to adhere for 15 min to poly-L-lysine-coated wells and then fixed by immersion in methanol for 10 min at −20°C. Alternatively, for LC3B labeling, Jurkat cells were incubated 10 min in 50 mM NH$_4$Cl after fixation in 4% paraformaldehyde for 10 min at RT, and then permeabilized in methanol for 10 min at −20°C. Fixed and permeabilized samples were washed for 5 min in PBS and incubated with primary antibodies overnight at 4°C, after blocking in 5% normal goat serum and 1% BSA for 1 h. Samples were washed for 5 min in PBS and incubated for 45 min at RT with Alexa-Fluor- 488-, Alexa-Fluor- 555-, and Alexa-Fluor-647-labeled secondary antibodies.

Confocal microscopy was carried out on a Zeiss LSM700 or a TCS SP8 Confocal laser scanning microscopy (Leica, Germany) using a 63× objective with pinholes opened to obtain 0.8 µm-thick sections. For the analyses shown in **Figures 2A, 3A,D, 4A** confocal microscopy imaging was carried out with a 0.2 Airy Unit pinhole which allows to obtain thinner optical section (less than 0.4 µm) from a single image. Detectors were set to detect an optimal signal below the saturation limits. Images were processed with Zen 2009 image software (Carl Zeiss, Jena, Germany).

The quantitative colocalization analysis was performed on median optical sections using ImageJ and JACoP plug-in to determine Mander's coefficient as previously described (Finetti et al., 2014). The ATG16L1 dispersion was quantified by measuring fluorescence intensity in concentric regions using ImageJ. Circular regions were centered on the point of ATG16L1 maximal intensity and designed proportionally to the cell size (inner circle, middle ring, and outer ring diameters, corresponding to 1/9, 1/4.5, and 1/2.25 of cell diameter, respectively) (Progida et al., 2010). Alternatively, ATG16L1 dispersion was measured using ImageJ by calculating the distance of ATG16L1$^+$ dots (identified using the same fluorescence threshold in control and IFT20KD cells in each experiments) from the centrosome (identified by pericentrin staining).

Autophagic Flux and LC3$^+$ Dot Number Measurement

To analyze the autophagic flux, 1×10^6 cells/sample were incubated in RPMI 1640 added with 7.5% BCS for 30 min at 37°C in the presence or absence of 40 µM chloroquine. Subsequently, cells were harvested and lysed in 1% Triton X-100 in 20 mM Tris–HCl pH 8.0, 150 mM NaCl in the presence of protease and phosphatase inhibitors, and processed for immunoblotting with anti-LC3B antibodies. Autophagy flux was calculated as

the difference in LC3-II levels, normalized to actin, between chloroquine-treated and untreated cells.

The number of LC3B$^+$ vesicles was determined by immunofluorescence microscopy. 1×10^5 cells/sample were incubated in RPMI 1640 added with 7.5% BCS for 30 min at 37°C with or without 40 µM chloroquine and allowed to adhere to poly-L-lysine-coated wells. Subsequently, the samples were fixed, permeabilized and stained as described above.

Membrane Fractionation

Cytosolic and membrane fractions were purified as previously described (Finetti et al., 2014). Jurkat cells (3×10^7/sample) were resuspended in 1 ml homogenization medium (0.25 M sucrose, 1 mM EDTA, 10 mM Tris–HCl pH 7.4) in the presence of protease and phosphatase inhibitors. The samples were homogenized by 10 pestle strokes through Dounce homogenization (tight Dounce homogenizer, Wheaton, United States) and 10 passages through a 26-gauge syringe needle. The homogenate was centrifuged at $3,000 \times g$ for 5 min at 4°C to remove nuclei and the supernatant was centrifuged at $65,000 \times g$ for 1 h at 4°C. The supernatant (cytosolic fraction) was collected, while the pellet (membrane fraction) was lysed in homogenization buffer containing protease and phosphatase inhibitors with 0.5% Triton, and centrifuged at $16,100 \times g$ for 20 min at 4°C to eliminate insoluble material. The same quantities of membrane protein-enriched supernatant and cytosolic fraction were analyzed by SDS-PAGE.

Statistical Analysis

GraphPad (Prism Software) was used to calculate mean values, standard deviation values and statistical significance. Values with Gaussian distribution were analyzed using Student's t test (paired or unpaired), one sample t test (theoretical mean = 1) or one-way ANOVA. Values without normal distribution were analyzed using Mann–Withney test or Kruskal–Wallis test. A level of $P < 0.05$ was considered statistically significant.

RESULTS

IFT20 Interacts Constitutively With ATG16L1 in T Cells

IFT20 interacts with ATG16L1 and colocalizes with this protein at intracellular vesicles in ciliated cells (Pampliega et al., 2013). The evidence that T cells share common regulators of vesicular trafficking with ciliated cells (Cassioli and Baldari, 2019) and that IFT20 deficiency is associated to impaired autophagic flux in T cells (Finetti et al., 2020) raises the question of whether IFT20 may interact with ATG16L1 also in non-ciliated T cells to promote autophagy. To address this issue, we performed co-immunoprecipitation experiments in Jurkat T cells, which showed that IFT20 interacts with ATG16L1 (**Figure 1A**). Consistent with this finding, IFT20 displayed partial colocalization with ATG16L1 in Jurkat T cells, as assessed by immunofluorescence (**Figure 1B**). The ability of IFT20 to interact with ATG16L1 was confirmed by *in vitro* GSH-Sepharose pull-down assays using an IFT20-GST fusion protein (**Figures 1C,D**).

Hence, similar to ciliated cells, IFT20 interacts with ATG16L1 in the non-ciliated T cell.

IFT20 is a small protein containing a single coiled-coil (CC) domain at its C-terminus (**Figure 1C**) that has been implicated in its heterodimerization with other CC domain-containing components of the IFT complex (Baker et al., 2003; Omori et al., 2008). To map the interaction of ATG16L1 on IFT20 we generated GST fusion proteins with the IFT20 CC domain (amino acid residues 74–132; CC IFT20) or the full-length protein lacking the CC domain (amino acid residues 1–73; ΔCC IFT20). The GST-pull down assays showed that ATG16L1 binds to IFT20 regardless of the presence of the CC-domain (**Figure 1D**). These results indicate that IFT20 interacts with ATG16L1 mostly through a molecular determinant localized within its unstructured region, potentially using its CC domain to couple ATG16L1 to sites of autophagosome formation.

To investigate the role of the CC domain in basal IFT20-dependent autophagy we generated Jurkat T cells transfectants expressing IFT20-GFP or a deletion mutant lacking the CC domain, fused to GFP (ΔCC IFT20-GFP) (**Figure 1E** and **Supplementary Figure 1A**). A similar construct encoding the isolated GFP-tagged CC domain was not expressed at detectable levels, likely due to low protein stability (data not shown). The impact of ΔCC IFT20 expression on the autophagic flux was assessed by immunoblot. Cells were either untreated or treated with chloroquine, which blocks the degradation of LC3-II by impairing autophagosome fusion with lysosomes (Mauthe et al., 2018). Immunoblot analysis with anti-LC3B antibodies showed that under basal conditions the autophagic flux was decreased in cells expressing ΔCC IFT20-GFP compared to controls expressing full-length IFT20-GFP (**Figure 1F**). This result was confirmed by immunofluorescence analysis of LC3$^+$ dots, which showed a decreased autophagic flux in ΔCC IFT20-GFP-expressing cells compared to controls expressing the full-length GFP fusion protein (**Figure 1G**). Hence, the pro-autophagic function of IFT20 requires its CC domain.

IFT20 Tethers ATG16L1 to Cellular Membranes

ATG16L1 is a cytoplasmic protein that is recruited to multiple cellular membranes which can serve as membrane sources for autophagosomes (Xiong et al., 2018). Although the mechanism of ATG16L1 recruitment to membranes is not fully understood, ATG16L1 has been reported to interact with the autophagy regulator FIP200 and with the phosphatidylinositol 3-phosphate [PI(3)P]-binding protein WIPI2. Both these interactions are functional to the association of ATG16L1 with isolation membranes, particularly at the endoplasmic reticulum, during autophagosome formation. ATG16L1 also interacts with the small GTPase Rab33 at the Golgi complex, SNX18/Rab11 at recycling endosomes, and the membrane coat protein clathrin at the plasma membrane, wherefrom it is transferred to the endocytic compartment (Itoh et al., 2008; Ravikumar et al., 2010; Gammoh et al., 2013).

The association of IFT20 with the Golgi apparatus and endocytic compartments (Finetti et al., 2009) and its ability to
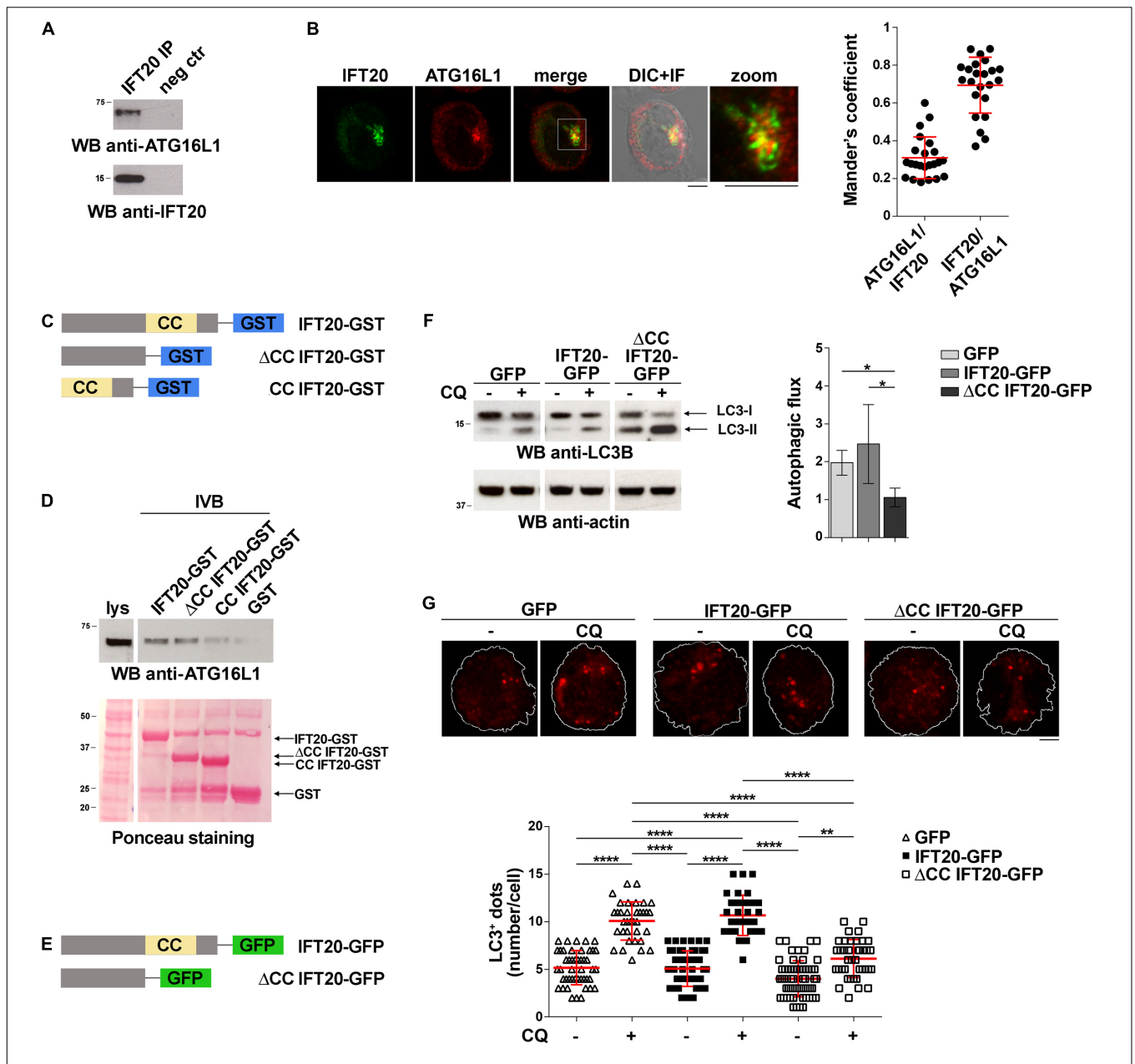
FIGURE 1 | IFT20 binds to ATG16L1 and promotes T cell autophagy through its CC domain. **(A)** Western blot (WB) analysis with anti-ATG16L1 antibodies of IFT20-specific immunoprecipitates from lysates of Jurkat T cells. A preclearing control (proteins bound to Protein-A–Sepharose before the addition of primary antibody) is included in each blot (neg ctr). The migration of molecular mass markers is indicated. The immunoblots shown are representative of at least 3 independent experiments. **(B)** Immunofluorescence analysis of IFT20 and ATG16L1 in Jurkat cells. Representative medial optical sections and overlay of immunofluorescence (IF) and differential interference contrast (DIC) images are shown (IF + DIC). The graph shows the quantification (using Mander's coefficient) of the weighted colocalization of IFT20 and ATG16L1 in Jurkat cells. The data are expressed as mean $\pm$ SD (23 cells/sample; $n = 3$). Scale bars: 5 μm. **(C)** Schematic representation of the GST fusion proteins with full-length IFT20 (IFT20-GST), or the full-length protein lacking the CC domain (ΔCC IFT20-GST) or the CC domain (CC IFT20-GST). The CC domain is highlighted as a yellow box. **(D)** Immunoblot analysis with anti-ATG16L1 antibodies of *in vitro*-binding assays carried out on post-nuclear supernatants of Jurkat cells using IFT20-GST, ΔCC IFT20-GST, and CC IFT20-GST fusion proteins, or GST as negative control. The Ponceau red staining of the same filter is shown to compare the levels of fusion proteins and GST used in the assay. The immunoblot shown is representative of three independent experiments. **(E)** Schematic representation of the GFP fusion protein with IFT20 (IFT20-GFP) or with the full-length protein lacking the CC domain (ΔCC IFT20-GFP). The CC domain is highlighted as a yellow box. **(F)** Immunoblot analysis of LC3B in lysates of Jurkat cells expressing GFP, IFT20-GFP, or ΔCC IFT20-GFP in the presence or absence of chloroquine (CQ, 40 μM). The migration of molecular mass markers is indicated. The graph shows the autophagic flux in Jurkat transfectants, calculated as the difference in the levels of LC3II/actin between CQ-treated and CQ-untreated samples (mean fold $\pm$ SD; one-way ANOVA; $n \geq 3$). **(G)** Immunofluorescence analysis of LC3B in Jurkat cells expressing GFP, IFT20-GFP, or ΔCC IFT20-GFP either untreated or treated for 30 min with chloroquine (CQ, 40 μM). The z-projection of maximum intensity and the quantification of the number of LC3$^+$ dots/cell are shown. At least 35 cells from three independent experiments were analyzed (mean $\pm$ SD; Kruskal–Wallis test). *$P < 0.05$; **$P < 0.01$; ****$P < 0.0001$.

interact with ATG16L1 (**Figure 1**) suggest a role for IFT20 in tethering ATG16L1 to endomembranes. To test this hypothesis we addressed the outcome of RNAi-mediated IFT20 depletion (IFT20KD; **Supplementary Figure 1B**) on the subcellular localization of ATG16L1. Immunofluorescence analysis showed that ATG16L1 was concentrated at a vesicular-like compartment in control cells, as previously reported in NIH3T3 cells (Itoh et al., 2008). The localization of ATG16L1 was altered to a significant extent in Jurkat cells stably knocked down for IFT20 expression, where it showed a dispersed pattern, as assessed by measuring the distance of ATG16L1$^+$ vesicles from the centrosome as well as by quantifying the fluorescence intensity in concentric cellular regions from the point of maximal intensity (**Figures 2A,B**; Progida et al., 2010). These results support the notion that IFT20 contributes to the vesicular localization of ATG16L1 in T cells.

To confirm this function of IFT20, the association of ATG16L1 with cellular membranes was addressed biochemically by immunoblot analysis of cytosolic and membrane fractions obtained from control and IFT20KD Jurkat cells. ATG16L1 was detected both in cytosolic and in membrane fractions. IFT20 deficiency resulted in a decrease in the amount of ATG16L1 associated with the membrane fractions (**Figure 2C**), suggesting that the loss of ATG16L1 compartmentalization observed by immunofluorescence in IFT20KD cells results from its release from cellular membranes to the cytosol.

To understand whether the CC domain of IFT20, which is required for the pro-autophagic function of IFT20 (**Figures 1F,G**) but not for ATG16L1 binding (**Figure 1D**), affects the subcellular localization of ATG16L1, we carried out an immunofluorescence analysis of ATG16L1 in Jurkat T cells expressing IFT20-GFP or the ΔCC IFT20-GFP mutant (**Figure 1E** and **Supplementary Figure 1A**). At variance with IFT20-GFP, which did not elicit any detectable effect, the absence of the CC domain resulted in a complete loss of the vesicular pattern of ATG16L1 (**Figure 2D**), similar to that observed in IFT20KD cells (**Figures 2A,B**). The alteration in the subcellular localization of ATG16L1 was paralleled by a diffuse staining throughout the cell of ΔCC IFT20-GFP, with only the centrosomal localization remaining unaffected (**Figure 2E**). This suggests that ΔCC IFT20-GFP acts in a dominant negative fashion to prevent the interaction of endogenous, membrane-associated IFT20 with ATG16L1. Importantly, the defect in ATG16L1 localization observed in IFT20KD cells was rescued by restoring IFT20 expression, while ΔCC-IFT20 was unable to correct this defect (**Figure 2F** and **Supplementary Figure 1C**). Hence IFT20 mediates the vesicular localization of ATG16L1 in T cells and this function maps to its CC domain.

IFT20 Is Required for the Association of ATG16L1 With the Golgi Apparatus

To identify the membrane compartment ATG16L1 associates with in T cells, we carried out a colocalization analysis of ATG16L1 with the Golgi complex, one of the most IFT20-enriched subcellular compartments (Follit et al., 2006; Finetti et al., 2009). A decrease in the colocalization of ATG16L1 with the Golgi marker giantin was observed in IFT20KD cells

compared to controls (**Figure 3A**), implicating IFT20 in the Golgi localization of ATG16L1.

IFT20 is known to associate with the Golgi apparatus through its interaction with the golgin GMAP210 (Follit et al., 2008). This interaction is mediated by the CC domain of GMAP210 (Follit et al., 2008; Zucchetti et al., 2019). To understand whether the IFT20-dependent association of ATG16L1 with the Golgi is mediated by GMAP210 we analyzed the subcellular localization of ATG16L1 in Jurkat cells knocked down for GMAP210 expression by RNA interference (**Supplementary Figure 1D**). Similar to IFT20KD cells, GMAP210KD cells showed a dispersed pattern of ATG16L1 staining, with a decrease in its association with the Golgi apparatus (**Figures 3B,C**). This was paralleled by a loss of IFT20 co-localization with the Golgi (**Figure 3D**), consistent with the ability of IFT20 to interact with GMAP210 in T cells (Galgano et al., 2017; Zucchetti et al., 2019).

To map the GMAP210 binding site on IFT20 we carried out pull-down assays using the IFT20-GST, ΔCC IFT20-GST, and CC IFT20-GST fusion proteins (**Figure 1C**). As expected, GMAP210 was found to interact with full-length IFT20 (**Figure 3E**). The CC domain of IFT20 was largely responsible for this interaction, as shown by the preferential binding to GMAP210 to the isolated CC domain compared to the fusion protein lacking the CC domain (**Figure 3E**). Consistent with this finding, the CC domain of IFT20 was essential for its association with the Golgi apparatus, as assessed in Jurkat cell transfectants expressing ΔCC IFT20-GFP (**Figure 3F**).

The Golgi apparatus has been identified as a source of autophagosomal membranes, contributing to phagophore elongation through ATG16L1 recruitment (Itoh et al., 2008; Staiano and Zappa, 2019). To understand whether the GMAP210-dependent, IFT20-mediated recruitment of ATG16L1 to the Golgi is implicated in the pro-autophagic function of IFT20 we measured the autophagic flux in GMAP210KD cells. Remarkably, GMAP210 deficiency did not impair basal autophagy, as assessed both by immunoblot and by immunofluorescence analysis of LC3 (**Figures 3G,H**). Hence, while IFT20 couples ATG16L1 to the Golgi in T cells through its CC domain-dependent interaction with GMAP210, the resulting Golgi association of ATG16L1 does not lead to autophagosome formation. Accordingly, the recruitment of BECLIN 1 to the Golgi complex is minimal in Jurkat cells, as assessed by immunofluorescence analysis of the colocalization of BECLIN 1 with the cis-Golgi marker GM130 (**Supplementary Figure 2**).

IFT20 Is Required for the Association of ATG16L1 With Early Endosomes

In T cells IFT20 is associated not only with the Golgi apparatus, but also with other endomembrane compartments, a major one being early endosomes, where it interacts with Rab5 (Finetti et al., 2014). Of relevance, Rab5 is a component of the macromolecular complex containing BECLIN 1 and the class III phosphatidylinositol-3 kinase VPS34 that regulates autophagosome formation (Ravikumar et al., 2008). An association of ATG16L1 with both early and recycling endosomes
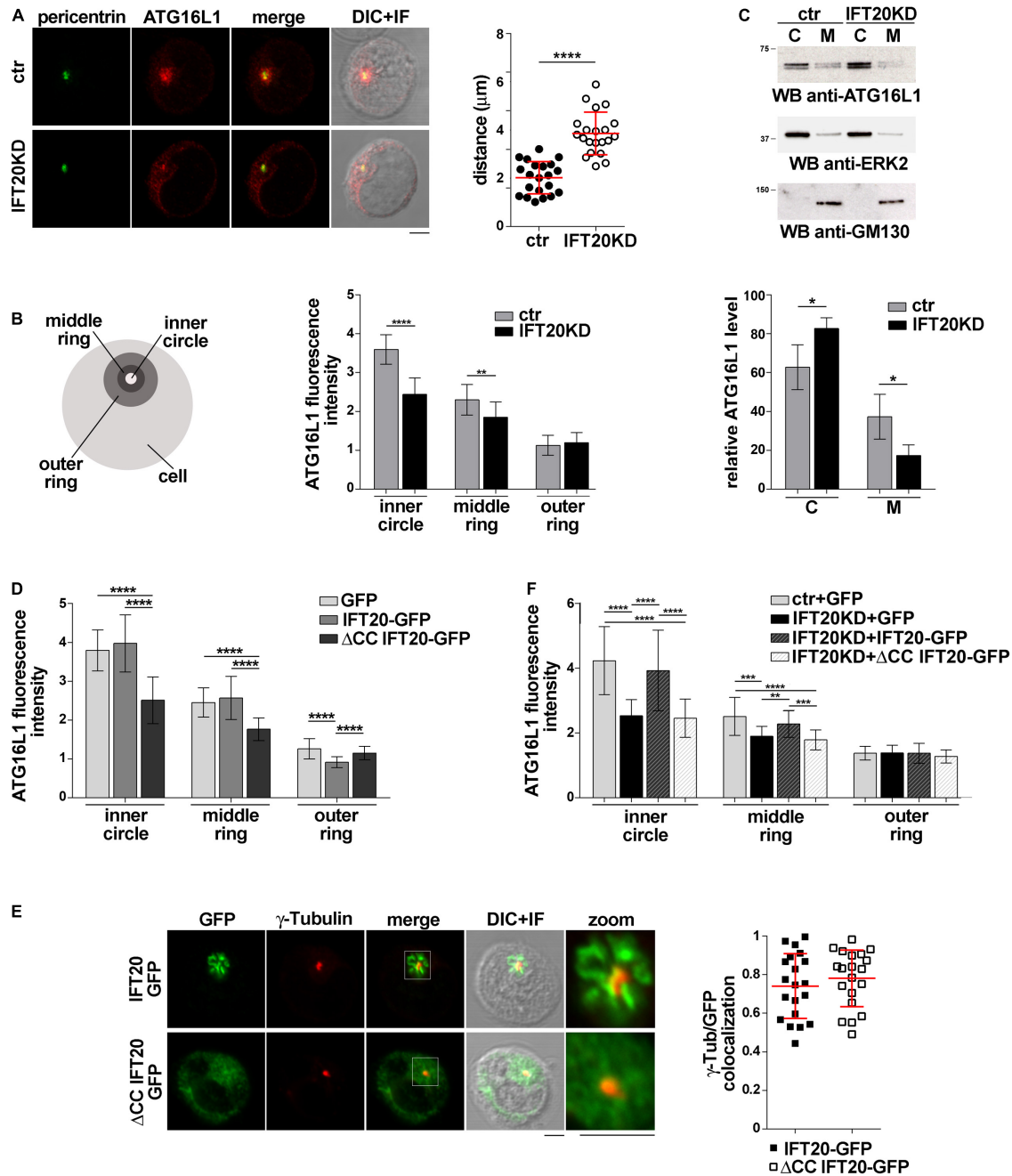
FIGURE 2 | IFT20 regulates the intracellular localization of ATG16L1. **(A,B)** Immunofluorescence analysis of ATG16L1 and the centrosomal protein pericentrin in control (ctr) and IFT20KD Jurkat cells. Representative medial optical sections and overlay of immunofluorescence and DIC images are shown (IF + DIC). Scale bars: 5 μm. **(A)** The graph shows the quantification of the distance of ATG16L1$^+$ vesicles from the centrosome (mean ± SD, 21 cells; $n = 3$; Student's t-test). **(B)** Histogram showing the quantification of fluorescence intensity in the concentric regions indicated in the scheme and defined from the point of ATG16L1 maximal intensity (mean ± SD, ≥ 20 cells/sample; $n = 3$; Mann–Whitney test). **(C)** Immunoblot analysis of ATG16L1 in cytosolic (C) and membrane (M) fractions purified from control and IFT20KD Jurkat cells. The cytosolic protein ERK2 and the *cis*-Golgi marker GM130 were used to assess the purity of cytosolic and membrane fractions, respectively. The migration of molecular mass markers is indicated. The histogram shows the quantification of the percentage of ATG16L1 in the cellular fractions obtained from 4 independent experiments (mean ± SD; Student's t-test). **(D)** Immunofluorescence analysis of ATG16L1 in GFP, IFT20-GFP, and ΔCC IFT20-GFP Jurkat transfectants. The histograms show the quantification of fluorescence intensity in the concentric regions described above (mean ± SD, ≥ 25 cells/sample; $n = 3$; Mann–Whitney test). **(E)** Quantification (using Mander's coefficient) of the weighted colocalization of γ-tubulin with GFP in medial confocal sections of IFT20-GFP or ΔCC IFT20-GFP expressing Jurkat cells (mean ± SD; ≥ 20 cells/line; $n = 3$). Representative images (medial optical sections and overlay DIC + IF) are shown. Scale bar: 5 μm. **(F)** Immunofluorescence analysis of ATG16L1 in control and IFT20KD cells transiently transfected with either empty vector (GFP), or the IFT20-GFP construct or the ΔCC IFT20-GFP construct. The graph shows the quantification of fluorescence intensity in the concentric regions described above (mean ± SD, ≥ 25 cells/sample; $n = 3$; Mann–Whitney test). *$P < 0.05$; **$P < 0.01$; ***$P < 0.001$; ****$P < 0.0001$.
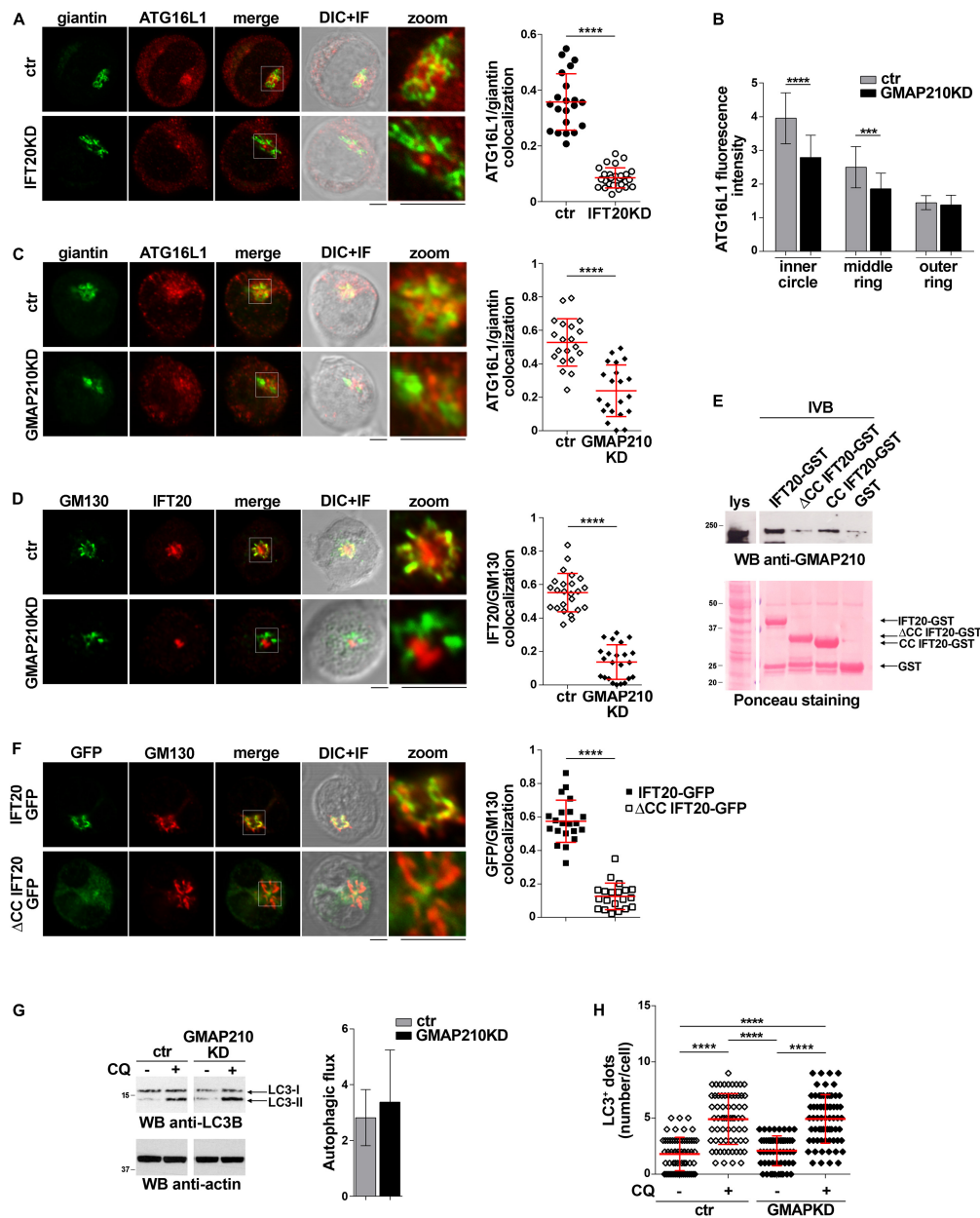
FIGURE 3 | IFT20 couples ATG16L1 to the Golgi through its CC domain-mediated interaction with GMAP210. **(A)** Quantification using Mander's coefficient of the weighted colocalization of ATG16L1 and the Golgi marker giantin in ctr and IFT20KD Jurkat cells ($\geq$ 21 cells/sample, n = 3; mean $\pm$ SD; Student's t-test). Representative images (medial optical sections and the overlay DIC + IF) are shown. Scale bar: 5 μm. **(B)** Quantification of fluorescence intensity of ATG16L1 in the concentric regions previously described (**Figure 2B**) in control and GMAP210KD cells (mean $\pm$ SD, $\geq$ 25 cells/sample; n = 3; Mann–Whitney test). **(C,D)** Immunofluorescence analysis of ATG16L1 and giantin **(C)** or IFT20 and the Golgi marker GM130 **(D)** in control and GMAP210KD cells. Representative medial optical sections and overlay of immunofluorescence (IF) and differential interference contrast (DIC) images are shown (IF + DIC). The graph shows the quantification (using Mander's coefficient) of the weighted colocalization of ATG16L1 and giantin **(C)** or IFT20 and GM130 **(D)**. The data are expressed as mean $\pm$ SD ($\geq$ 20 cells/sample; n = 3; Mann–Whitney test). Scale bars: 5 μm. **(E)** Immunoblot analysis with anti-GMAP210 antibodies of *in vitro*-binding assays carried out on post-nuclear supernatants of Jurkat cells using IFT20-GST, ΔCC IFT20-GST and CC IFT20-GST fusion proteins, or GST as negative control. The Ponceau red staining of the same filter is shown to compare the levels of fusion proteins and GST used in the assay. The immunoblot shown is representative of three independent experiments. **(F)** Quantification (using Mander's coefficient) of the weighted colocalization of the *cis*-Golgi marker GM130 with GFP in medial confocal sections of IFT20-GFP or ΔCC IFT20-GFP expressing Jurkat cells (mean $\pm$ SD; $\geq$ 20 cells/line; n = 3; Mann–Whitney test). Representative images (medial optical sections and overlay DIC + IF) are shown. Scale bar: 5 μm. **(G)** Immunoblot analysis of LC3B in lysates of control or GMAP210KD cells in the presence or absence of chloroquine (CQ, 40 μM). The migration of molecular mass markers is indicated. The histograms show the autophagic flux calculated as the difference in the levels of LC3II/actin between CQ-treated and CQ-untreated samples (mean fold $\pm$ SD; Student's t-test; $n \geq$ 3). **(H)** Quantification of the number of LC3^{+} dots/cell in control or GMAP210KD cells either untreated or treated for 30 min with chloroquine (CQ, 40 μM). At least 35 cells from three independent experiments were analyzed (mean $\pm$ SD; Kruskal–Wallis test). **P < 0.01; ***P < 0.001; ****P < 0.0001.
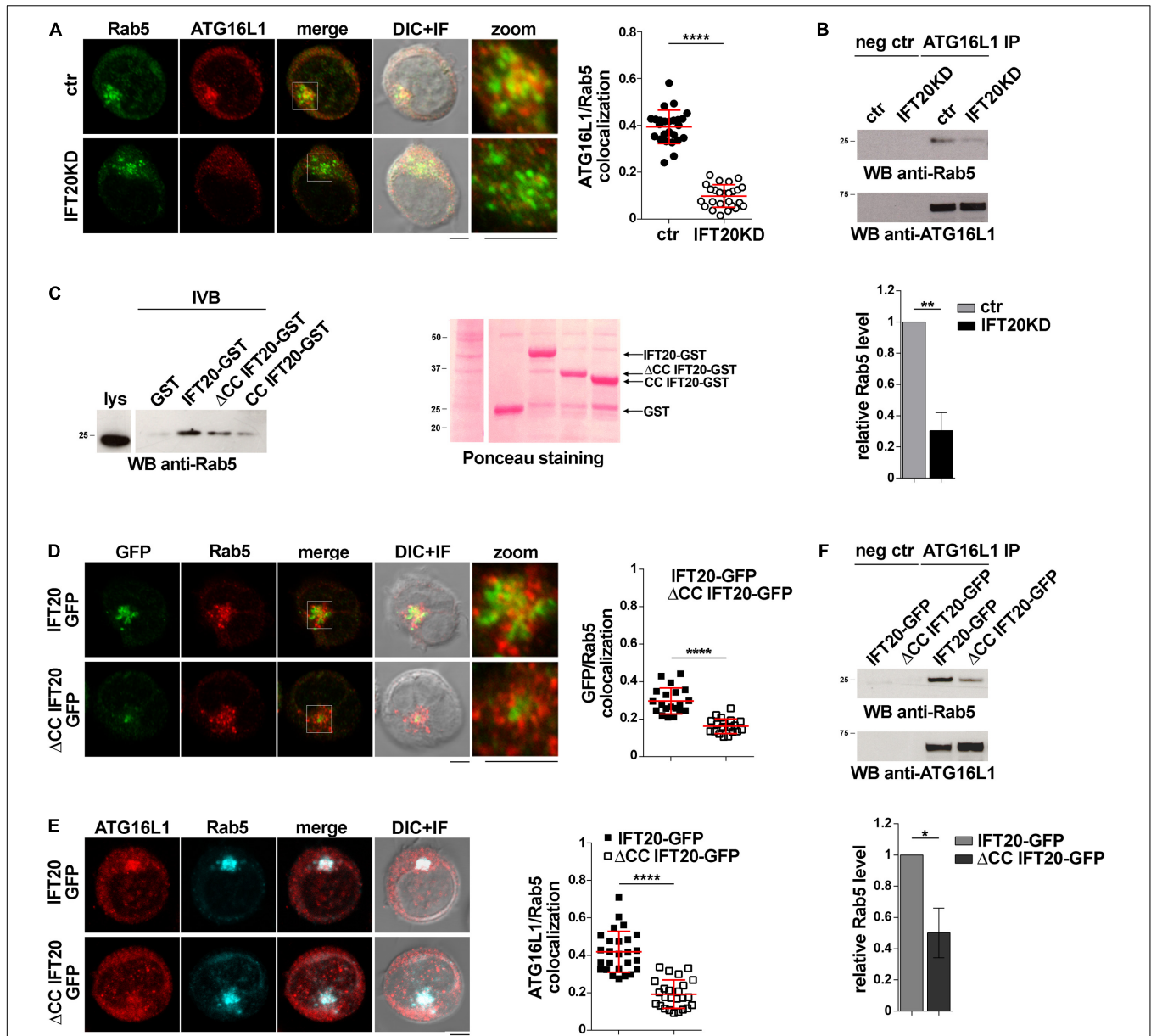
FIGURE 4 | IFT20 couples ATG16L1 to early endosomes through interaction with Rab5. **(A)** Immunofluorescence analysis of ATG16L1 and Rab5 GFP in control and IFT20KD Jurkat cells. Representative medial optical sections and overlay of immunofluorescence and DIC images are shown (IF + DIC). Scale bar: 5 μm. The graph shows the quantification of the weighted colocalization (Mander's coefficient) of ATG16L1 and the early endosome marker Rab5 in ctr and IFT20KD Jurkat cells (= 25 cells/sample, n = 3; mean ± SD; Student's t-test). **(B)** Immunoblot analysis with anti-Rab5 antibodies of ATG16L1-specific immunoprecipitates from lysates of control and IFT20KD Jurkat cells. Preclearing controls are included in each blot (neg ctr). Tested proteins show comparable expression in total cell lysate from ctr and IFT20KD Jurkat cells (**Supplementary Figures 3A,B**). The migration of molecular mass markers is indicated. The quantification of the relative protein expression normalized to ATG16L1 (mean fold ± SD; ctr value = 1) is reported for each blot (n = 3; mean ± SD; Student's t-test). **(C)** Immunoblot analysis with anti-Rab5 antibodies of *in vitro*-binding assays carried out on post-nuclear supernatants of Jurkat cells using IFT20-GST, ΔCC IFT20-GST, and CC IFT20-GST fusion proteins, or GST as negative control. The Ponceau red staining of the same filter is shown to compare the levels of fusion proteins and GST used in the assay. The immunoblot shown is representative of three independent experiments. **(D)** Immunofluorescence analysis of GFP and Rab5 in Jurkat cells expressing IFT20-GFP and ΔCC IFT20-GFP. The graph shows the quantification using Mander's coefficient of the weighted colocalization of GFP and Rab5 in Jurkat transfectants reported as mean value/cell calculated on individual Rab5+ dot (= 20 cells/sample, n = 3; mean ± SD; Student's t-test). **(E)** Immunofluorescence analysis of ATG16L1 and Rab5 in IFT20-GFP and ΔCC IFT20-GFP Jurkat transfectants. The graph shows the quantification of the weighted colocalization (Mander's coefficient) of ATG16L1 and Rab5 (≥ 25 cells/sample, n = 3; mean ± SD; Student's t-test) in Jurkat transfectants. Representative medial optical sections and overlay of immunofluorescence and DIC images are shown (IF + DIC). Scale bar: 5 μm. **(F)** Immunoblot analysis with anti-Rab5 antibodies of ATG16L1-specific immunoprecipitates from lysates of Jurkat cells expressing IFT20-GFP or ΔCC IFT20-GFP. Preclearing controls are included in each blot (neg ctr). The migration of molecular mass markers is indicated. The quantification of Rab5 levels normalized to ATG16L1 (mean fold ± SD; ctr value = 1) is shown (n = 3; mean ± SD; Student's t-test). $^{**}P < 0.01$; $^{***}P < 0.001$; $^{****}P < 0.0001$.

has been reported in other cell types (Ravikumar et al., 2010; Puri et al., 2013; Fraser et al., 2019), suggesting the possibility that IFT20 may exploit its interaction with Rab5 to recruit ATG16L1 to early endosomes to promote autophagy.

To investigate whether ATG16L1 associates with early endosomes in T cells and whether IFT20 is required for its localization, we carried out a colocalization analysis of ATG16L1 and Rab5 in control and IFT20KD T cells. Interestingly, we found that a pool of ATG16L1 was associated with Rab5$^+$ endosomes in control cells, as reported for glial cells (Fraser et al., 2019). IFT20 depletion resulted in a significant decrease in the colocalization of ATG16L1 with Rab5 (**Figure 4A**). Additionally, ATG16L1 was found to interact with Rab5 in co-immunoprecipitation experiments (**Figure 4B**). This interaction was impaired in IFT20 KD cells (**Figure 4B**).

To map the interaction of IFT20 with Rab5 we carried out pull-down assays using the IFT20-GST, CC IFT20-GST, and ΔCC IFT20-GST fusion proteins (**Figure 1C**). Rab5 interacted both with the GST-tagged isolated CC domain and with the fusion protein lacking the CC domain, indicating that molecular determinants mapping to different parts of IFT20 contribute to its ability to bind Rab5 (**Figure 4C**). Interestingly, the CC domain of IFT20 was found to be required for its association with early endosomes, as assessed in Jurkat cell transfectants expressing ΔCC IFT20-GFP and stained for Rab5 (**Figure 4D**). Additionally, ATG16L1 co-localization and interaction with Rab5 was compromised in these cells (**Figures 4E,F**). These results indicate that, by interacting with Rab5 and ATG16L1 using both its unstructured portion and its CC domain, IFT20 promotes the association of ATG16L1 with early endosomes.

IFT20 Is Required for the Interaction of ATG16L1 With Autophagy Regulators

The autophagy regulator BECLIN 1 assists the localization of ATG16L1 to the sites of autophagosome formation both indirectly and directly. BECLIN 1 forms a complex with VPS34, which induces a local increase in PI(3)P at the isolation membrane (Funderburk et al., 2010), leading to ATG16L1 recruitment through binding to the PI(3)P-binding adaptor WIPI2 (Dooley et al., 2014). Additionally, ATG16L1 interacts with BECLIN 1 in a complex that includes the gap junction protein connexin 43 (Bejarano et al., 2014). Compartment-specific interactors, such as Rab5 for early endosomes in HeLa cells (Ravikumar et al., 2008; Otomo et al., 2011), promote local autophagosome formation by recruiting BECLIN 1.

The finding that IFT20 is required for the association of ATG16L1 with membrane compartments in T cells raises the question of whether IFT20 is implicated in the formation of the autophagy-regulating complexes in which ATG16L1 participates. Since the IFT20-dependent recruitment of ATG16L1 to the Golgi apparatus does not appear to contribute to its pro-autophagic function in T cells (**Figures 3G,H**), we focused on early endosomes. In particular, we addressed the role of IFT20 in the interaction of ATG16L1 with BECLIN 1 at this membrane compartment. Similar to other cell types (Bejarano et al., 2014), ATG16L1 was found to co-immunoprecipitate and

co-localize with BECLIN 1 in T cells. This association was impaired in IFT20KD T cells (**Figures 5A,B**). Conversely, IFT20 deficiency did not affect the ability of ATG16L1 to interact with its downstream autophagy-regulating partner ATG5 (**Figure 5C**), which is covalently bound to ATG12 (Mizushima et al., 1998). Additionally, neither the interaction of BECLIN 1 with Rab5 (**Figure 5D**) nor their co-localization (**Figure 5E**) were affected by IFT20 deficiency. Accordingly, PI(3)P production at early endosomes was comparable to controls in IFT20KD cells, as assessed by quantifying the co-localization of Rab5 with GFP in cells transiently transfected with a GFP-tagged reporter construct encoding the tandem FYVE domains of hepatocyte growth factor-regulated tyrosine kinase substrate, which specifically interacts with PI(3)P (**Figure 5F**). Together, these results suggest that IFT20 is required for the recruitment of the ATG16L1-ATG5-ATG12 complex to early endosomes that have been tagged for autophagosome formation by Rab5-associated BECLIN 1.

ATG16L1 is involved in determining the site of LC3 lipidation, functioning as a scaffold to recruit the ATG12-ATG5 conjugating enzyme and LC3 to allow for the transfer reaction of LC3 from ATG3 to phosphatidylethanolamine at the phagophore membrane (Hanada et al., 2007; Fujita et al., 2008). The potential impact of IFT20 depletion on the ability of ATG16L1 to interact with LC3 was assessed in co-immunoprecipitation experiments. ATG16L1 was found to co-immunoprecipitate with LC3-I (**Figure 6A**). This suggests that the pool of ATG16L1 recruited to early endosomes by IFT20 might in turn recruit LC3-I to promote its local cleavage and lipidation to LC3-II. In support of this notion, the interaction of ATG16L1 with LC3-I was significantly impaired in IFT20-deficient T cells (**Figure 6A**). To further address this issue cells were co-stained for LC3 and ATG16L1. IFT20 deficiency resulted in a decrease in the co-localization of ATG16L1 with LC3$^+$ dots (**Figure 6B**). As previously reported, the number of LC3$^+$ dots was higher in IFT20KD cells due to their impaired ability to clear autolysosomes (Finetti et al., 2020). Importantly, a decrease in the co-localization of LC3 with Rab5 was also observed under these conditions (**Figure 6C**). Taken together, these results indicate that IFT20 participates in autophagosome formation by targeting ATG16L1 and its partners ATG5-ATG12 to Rab5$^+$ and BECLIN-1$^+$ vesicles, allowing for the recruitment of LC3 to promote the local generation of isolation membranes at early endosomes.

DISCUSSION

We have previously reported that IFT20 indirectly promotes T cell autophagy by regulating the mannose-6-P receptor-dependent transport of acid hydrolases to lysosomes (Finetti et al., 2020). Based on the implication of IFT20 in autophagosome formation in ciliated cells (Pampliega et al., 2013), here we investigated the potential direct implication of IFT20 in this process in the non-ciliated T cell. We show that, under basal conditions, IFT20 interacts with the autophagy regulator ATG16L1 and recruits it to both the Golgi apparatus and early endosomes. For this function IFT20 exploits its CC domain to bind the golgin GMAP210 at the Golgi, and
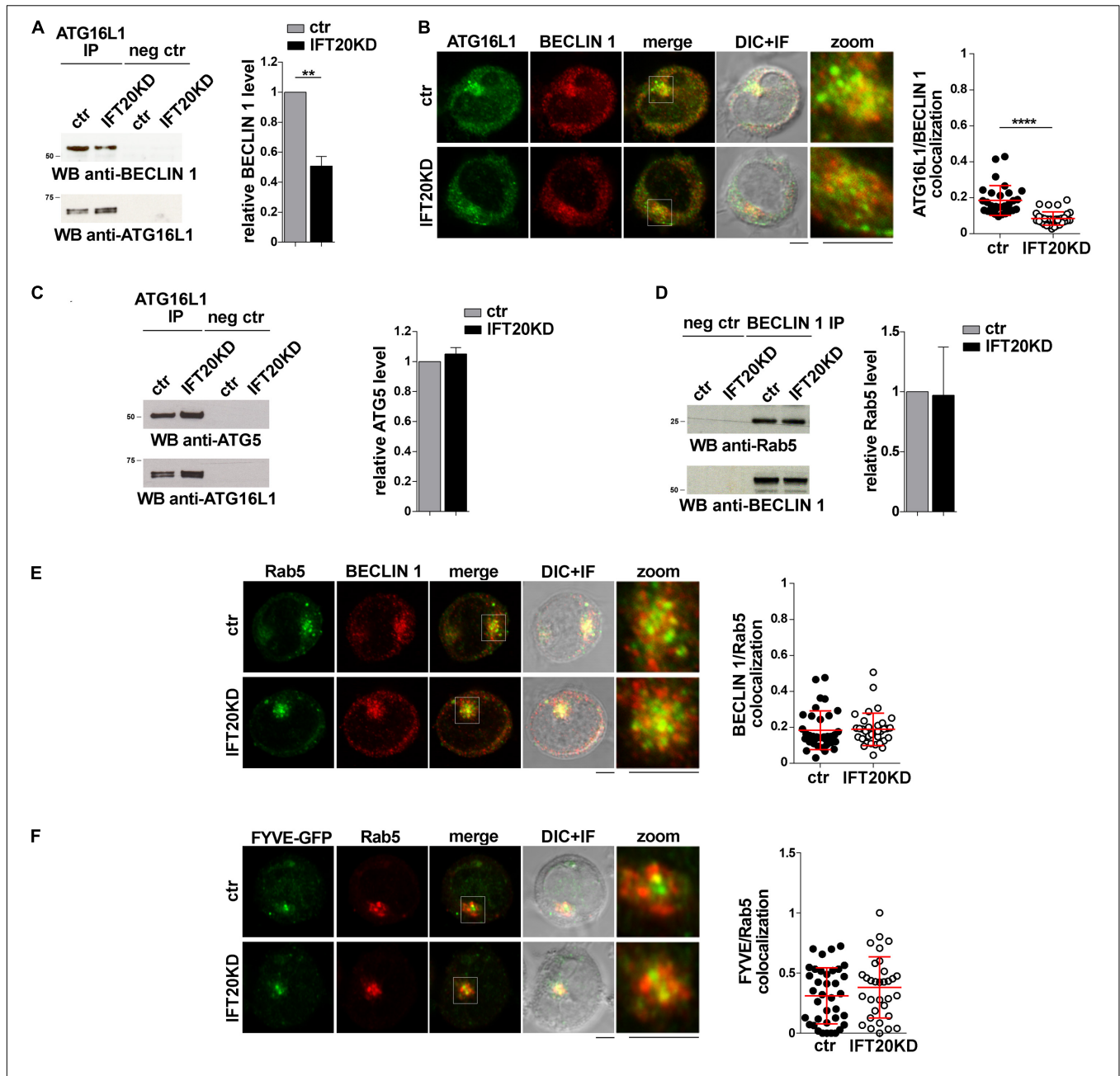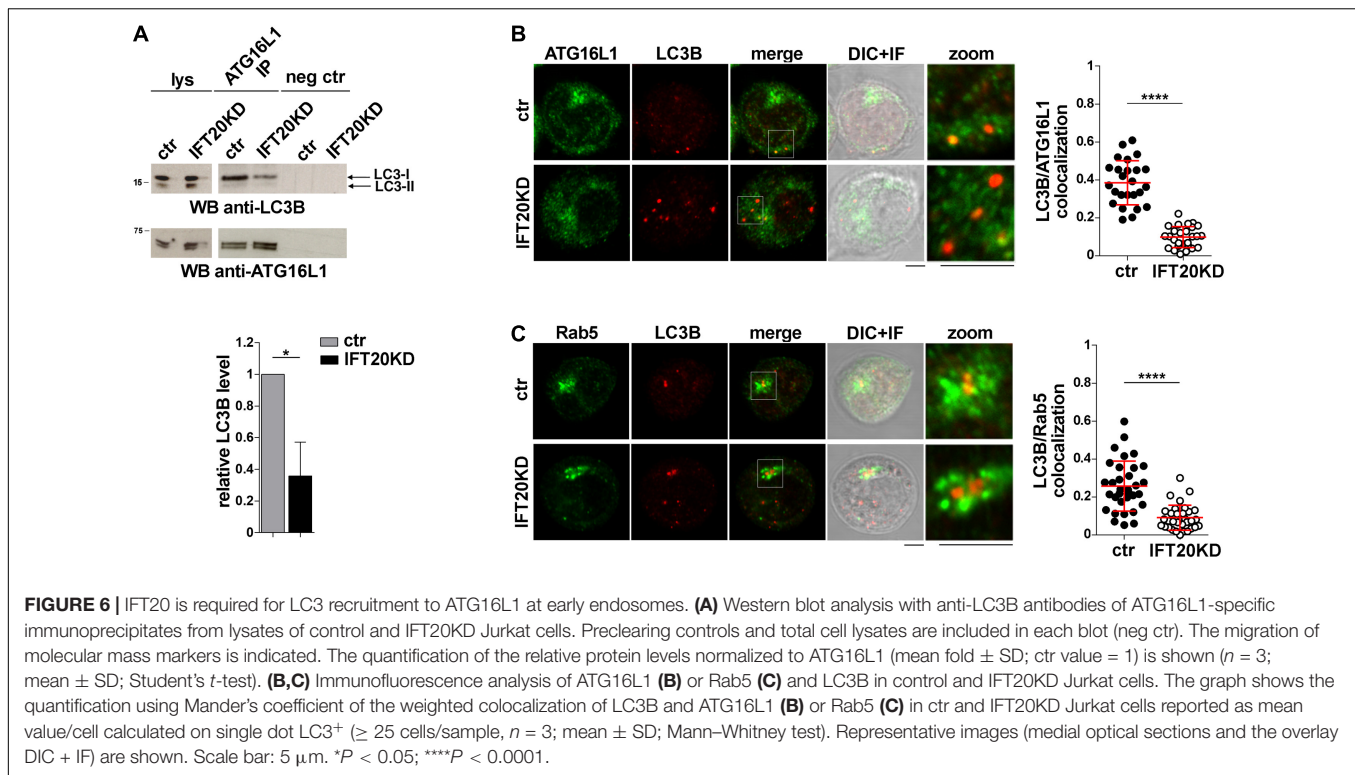
FIGURE 5 | IFT20 recruits ATG16L1 to early endosomes tagged for autophagosome formation. **(A)** Immunoblot analysis with BECLIN 1 antibodies of ATG16L1-specific immunoprecipitates from lysates of control and IFT20KD Jurkat cells. Preclearing controls are included in each blot (neg ctr). Tested proteins show comparable expression in total cell lysate from ctr and IFT20KD Jurkat cells (**Supplementary Figures 3A,C**). The migration of molecular mass markers is indicated. The quantification of the relative protein expression normalized to ATG16L1 (mean fold ± SD; ctr value = 1) is reported for each blot (n = 3; mean ± SD; Student's t-test). **(B)** Quantification (using Mander's coefficient) of the weighted colocalization of ATG16L1 with BECLIN 1 in medial confocal sections of control and IFT20KD Jurkat cells (mean ± SD; ≥ 30 cells/line; n = 3; Mann–Whitney test). Representative images (medial optical sections and overlay DIC + IF) are shown. Scale bar: 5 μm. **(C)** Immunoblot analysis with ATG5 antibodies of ATG16L1-specific immunoprecipitates from lysates of control and IFT20KD Jurkat cells. Preclearing controls are included in each blot (neg ctr). Tested proteins show comparable expression in total cell lysate from ctr and IFT20KD Jurkat cells (**Supplementary Figures 3A,D**). The migration of molecular mass markers is indicated. The quantification of the relative protein expression normalized to ATG16L1 (mean fold ± SD; ctr value = 1) is reported for each blot (n = 3; mean ± SD). **(D)** Immunoblot analysis with Rab5 antibodies of BECLIN 1-specific immunoprecipitates from lysates of control and IFT20KD Jurkat cells. Preclearing controls are included in each blot (neg ctr). Tested proteins show comparable expression in total cell lysate from ctr and IFT20KD Jurkat cells (**Supplementary Figures 3B,C**). The migration of molecular mass markers is indicated. The quantification of the relative protein expression normalized to ATG16L1 (mean fold ± SD; ctr value = 1) is reported for each blot (n = 3; mean ± SD). **(E,F)** Immunofluorescence analysis of BECLIN 1 and Rab5 **(E)** or FYVE-GFP and Rab5 **(F)** in control and IFT20KD Jurkat cells. Representative medial optical sections and overlay of immunofluorescence and DIC images are shown (IF + DIC). Scale bar: 5 μm. The graphs show the quantification of the weighted colocalization (Mander's coefficient) of BECLIN 1 **(E)** or FYVE-GFP **(F)** and Rab5 in ctr and IFT20KD Jurkat cells (mean ± SD; ≥ 32 cells/line; n = 3; Mann–Whitney test). ****P < 0.0001.

FIGURE 6 | IFT20 is required for LC3 recruitment to ATG16L1 at early endosomes. **(A)** Western blot analysis with anti-LC3B antibodies of ATG16L1-specific immunoprecipitates from lysates of control and IFT20KD Jurkat cells. Preclearing controls and total cell lysates are included in each blot (neg ctr). The migration of molecular mass markers is indicated. The quantification of the relative protein levels normalized to ATG16L1 (mean fold ± SD; ctr value = 1) is shown ($n = 3$; mean ± SD; Student's t-test). **(B,C)** Immunofluorescence analysis of ATG16L1 **(B)** or Rab5 **(C)** and LC3B in control and IFT20KD Jurkat cells. The graph shows the quantification using Mander's coefficient of the weighted colocalization of LC3B and ATG16L1 **(B)** or Rab5 **(C)** in ctr and IFT20KD Jurkat cells reported as mean value/cell calculated on single dot LC3$^+$ ($\geq$ 25 cells/sample, $n = 3$; mean ± SD; Mann–Whitney test). Representative images (medial optical sections and the overlay DIC + IF) are shown. Scale bar: 5 μm. *$P < 0.05$; ****$P < 0.0001$.

molecular determinants mapping to both the CC domain and the unstructured domain to bind the small GTPase Rab5 at early endosomes. We provide evidence that the IFT20-dependent ATG16L1 localization to early endosomes, but not to the Golgi apparatus, results in the local formation of autophagosomes downstream of BECLIN 1 recruitment and PI(3)P production. The results highlight a dual role of IFT20 in basal T cell autophagy.

IFT20 has been previously demonstrated to regulate both basal and starvation-induced autophagy in ciliated cells (Pampliega et al., 2013). Our data, implicating IFT20 in basal T cell autophagy, underscore the notion that the ciliogenesis machinery is exploited by the non-ciliated T cell beyond immune synapse assembly. In support of this notion, we have recently demonstrated that IFT20 participates in lysosome biogenesis, a function that we found to be shared by ciliated cells (Finetti et al., 2020). The autophagy-related mechanism appears, however, to differ, at least in part. In ciliated cells the IFT system is required for the transport of autophagy regulators – including VPS34, ATG14, ATG16L1, and ATG7 – to the base of the cilium (Pampliega et al., 2013). Additionally, IFT20 co-localizes with ATG16L1 at small Golgi-proximal vesicles that undergo trafficking to the cilium upon cell starvation, independently of other components of the IFT system (Pampliega et al., 2013). Here we show that IFT20 co-localizes with ATG16L1 at the Golgi apparatus. Additionally, the IFT20-dependent Golgi localization of ATG16L1 does not appear relevant to the pro-autophagic function of IFT20, at least under basal conditions. Indeed, untethering IFT20 from the Golgi through depletion of its interactor GMAP210 did not compromise autophagy,

despite the dissipation of ATG16L1 away from the Golgi. The Golgi apparatus has been identified as one of the membrane sources for phagophore elongation in other cell types, with ATG16L1 promoting the local recruitment and lipidation of LC3 (Fujita et al., 2008; Davis et al., 2017). Our data suggest that other ATG16L1 pools, recruited to the Golgi apparatus by alternative interactors, such as Rab33 (Itoh et al., 2008), might contribute to the local formation of autophagosomes. However, we have detected minimal co-localization of BECLIN 1 with the Golgi in T cells. As an alternative possibility, Golgi-associated ATG16L1 may play autophagy-independent functions in these cells, as recently reported in *Dictyostelium discoideum* (Karow et al., 2020).

We found that, as opposed to the Golgi, early endosomes are sites of autophagosome formation in T cells, as shown by the local accumulation of BECLIN 1, PI(3)P, ATG16L1, and LC3. Interestingly, while IFT20 appears dispensable for the association of a functional class III PI3-K complex with early endosomes, it is essential for the recruitment of ATG16L1 to this location. PI(3)P is known to promote the WIPI2-dependent association of ATG16L1 with sites of autophagosome formation (Dooley et al., 2014). However, additional interactors participate in its targeting to specific membrane compartments, including Rab33 at the Golgi apparatus, SNX18/Rab11 at recycling endosomes and clathrin at the plasma membrane (Itoh et al., 2008; Ravikumar et al., 2010; Knævelsrud et al., 2013; Puri et al., 2013). Here we identify Rab5 as an early endosome-specific binding partner of ATG16L1 in T cells, which may account for the association of ATG16L1 with early endosomes reported for other cell types (Fraser et al., 2019). Of note, Rab5 participates in a complex

with BECLIN 1 and VPS34 (Ravikumar et al., 2008). Our results implicate Rab5 not only in marking early endosomes as sites of autophagosome formation by promoting the VPS34-dependent production of PI(3)P, but also in assisting the subsequent recruitment and/or stabilization of ATG16L1 at these sites using IFT20 as an adaptor.

Our data provide evidence that the association of IFT20 with both the Golgi apparatus and early endosomes is mediated by compartment-specific interactors, namely GMAP210, as previously reported (Follit et al., 2008) and Rab5, respectively. Both these interactions map to the CC domain of IFT20, as shown both in pull-down assays and by co-localization analysis of cells expressing an IFT20 deletion mutant lacking the CC domain. The site of interaction of IFT20 on GMAP210 has been mapped to the CC domain of the latter (Follit et al., 2008; Zucchetti et al., 2019). Hence GMAP210 and IFT20 heterodimerize through their respective CC domain, consistent with the function of CC domains in establishing protein-protein interactions (Mason and Arndt, 2004). IFT20 exploits its CC domain to also interact with Rab5, however, the pull-down assays with the GST-tagged IFT20 construct lacking the CC domain show that the unstructured domain also binds Rab5, indicating the cooperation of multiple molecular determinants of IFT20 in this interaction. Of note, at variance with its compartment-specific binding partners, the interaction of IFT20 with ATG16L1 is CC domain-independent and maps to the unstructured N-terminal portion of the protein. While the only protein-protein interaction domain of IFT20 is its CC domain, which is used for binding IFT54 and IFT57 within the IFT complex (Baker et al., 2003; Omori et al., 2008), IFT20 is able to recognize and bind a number of proteins at the Golgi apparatus for sorting and targeting to the ciliary membrane, as exemplified by rhodopsin, opsin, and polycystin-2 (Follit et al., 2006; Keady et al., 2011). Hence, similar to these interactors, ATG16L1 might bind directly or indirectly to a molecular determinant within the IFT20 N-terminus that remains to be identified.

Longevity is a key feature of both naive and memory T cells as it ensures the maintenance of the immune repertoire as well as long-lasting protection from pathogens toward which the organism has mounted an effective immune response. Basal autophagy is one of the main mechanisms that underlie this extended T cell survival (Pua et al., 2007; Kovacs et al., 2012; Xu et al., 2014). Our finding of a dual role of IFT20 in autophagy, i.e., promoting autophagosome formation by recruiting ATG16L1 at early endosomes, and allowing for the degradation of the autolysosome contents by controlling lysosome biogenesis

(Finetti et al., 2020), highlights IFT20 as a key player in T cell homeostasis.

DATA AVAILABILITY STATEMENT

The raw data supporting the conclusions of this article will be made available by the authors, without undue reservation.

AUTHOR CONTRIBUTIONS

All authors listed have made a substantial, direct and intellectual contribution to the work, and approved it for publication. FF and CB wrote the manuscript. FF prepared the figures.

FUNDING

ACKNOWLEDGMENTS

SUPPLEMENTARY MATERIAL

The Supplementary Material for this article can be found online at: https://www.frontiersin.org/articles/10.3389/fcell.2021.634003/full#supplementary-material

REFERENCES

Baker, S. A., Freeman, K., Luby-Phelps, K., Pazour, G. J., and Besharse, J. C. (2003). IFT20 links kinesin ii with a mammalian intraflagellar transport complex that is conserved in motile flagella and sensory cilia. *J. Biol. Chem.* 278, 34211–34218. doi: 10.1074/jbc.M300156200

Bejarano, E., Yuste, A., Patel, B., Randy, R. F., Spray, D. C., and Cuervo, A. M. (2014). Connexins modulate autophagosome biogenesis. *Nat. Cell Biol.* 16, 401–414. doi: 10.1038/ncb2934

Cassioli, C., and Baldari, C. T. (2019). A ciliary view of the immunological synapse. *Cells* 8:789. doi: 10.3390/cells8080789

Davis, S., Wang, J., and Ferro-Novick, S. (2017). Developmental cell review crosstalk between the secretory and autophagy pathways regulates autophagosome formation. *Dev. Cell* 41, 23–32. doi: 10.1016/j.devcel.2017.03.015

Dikic, I., and Elazar, Z. (2018). Mechanism and medical implications of mammalian autophagy. *Nat. Rev. Mol. Cell Biol.* 19, 349–364. doi: 10.1038/s41580-018-0003-4

Dooley, H. C., Razi, M., Polson, H. E. J., Girardin, S. E., Wilson, M. I., and Tooze, S. A. (2014). WIPI2 links LC3 conjugation with PI3P, autophagosome formation, and pathogen clearance by recruiting Atg12-5-16L1. *Mol. Cell* 55, 238–252. doi: 10.1016/j.molcel.2014.05.021

Finetti, F., Cassioli, C., Cianfanelli, V., Onnis, A., Paccagnini, E., Kabanova, A., et al. (2020). The intraflagellar transport protein IFT20 controls lysosome biogenesis by regulating the post-Golgi transport of acid hydrolases. *Cell Death Differ.* 27, 310–328. doi: 10.1038/s41418-019-0357-y

Finetti, F., Paccani, S. R., Riparbelli, M. G., Giacomello, E., Perinetti, G., Pazour, G. J., et al. (2009). Intraflagellar transport is required for polarized recycling of the TCR/CD3 complex to the immune synapse. *Nat. Cell Biol.* 11, 1332–1339. doi: 10.1038/ncb1977

Finetti, F., Paccani, S. R., Rosenbaum, J., and Baldari, C. T. (2011). Intraflagellar transport: a new player at the immune synapse. *Trends Immunol.* 32, 139–145. doi: 10.1016/j.it.2011.02.001

Finetti, F., Patrussi, L., Masi, G., Onnis, A., Galgano, D., Lucherini, O. M., et al. (2014). Specific recycling receptors are targeted to the immune synapse by the intraflagellar transport system. *J. Cell Sci.* 127, 1924–1937. doi: 10.1242/jcs.139337

Follit, J. A., San Agustin, J. T., Xu, F., Jonassen, J. A., Samtani, R., Lo, C. W., et al. (2008). The Golgin GMAP210/TRIP11 anchors IFT20 to the Golgi complex. *PLoS Genet.* 4:e1000315. doi: 10.1371/journal.pgen.1000315

Follit, J. A., Tuft, R. A., Fogarty, K. E., and Pazour, G. J. (2006). The intraflagellar transport protein IFT20 is associated with the golgi complex and is required for cilia assembly. *Mol. Biol. Cell* 17, 3781–3792. doi: 10.1091/mbc.e06-02-0133

Fraser, J., Simpson, J., Fontana, R., Kishi−Itakura, C., Ktistakis, N. T., and Gammoh, N. (2019). Targeting of early endosomes by autophagy facilitates EGFR recycling and signalling. *EMBO Rep.* 20:e47734. doi: 10.15252/embr.201947734

Fujita, N., Itoh, T., Omori, H., Fukuda, M., Noda, T., and Yoshimori, T. (2008). The Atg16L complex specifies the site of LC3 lipidation for membrane biogenesis in autophagy. *Mol. Biol. Cell* 19, 2092–2100. doi: 10.1091/mbc.E07-12-1257

Funderburk, S. F., Wang, Q. J., and Yue, Z. (2010). Beclin 1-VPS34 complex-at the crossroads of autophagy and beyond. *Trends Cell Biol.* 20, 355–362. doi: 10.1016/j.tcb.2010.03.002

Galgano, D., Onnis, A., Pappalardo, E., Galvagni, F., Acuto, O., and Baldari, C. T. (2017). The T cell IFT20 interactome reveals new players in immune synapse assembly. *J. Cell Sci.* 130, 1110–1121. doi: 10.1242/jcs.200006

Gammoh, N., Florey, O., Overholtzer, M., and Jiang, X. (2013). Interaction between FIP200 and ATG16L1 distinguishes ULK1 complex-dependent and-independent autophagy. *Nat. Struct. Mol. Biol.* 20, 144–149. doi: 10.1038/nsmb.2475

Hanada, T., Noda, N. N., Satomi, Y., Ichimura, Y., Fujioka, Y., Takao, T., et al. (2007). The Atg12-Atg5 conjugate has a novel E3-like activity for protein lipidation in autophagy. *J. Biol. Chem.* 282, 37298–37302. doi: 10.1074/jbc.C700195200

Hubbard, V. M., Valdor, R., Patel, B., Singh, R., Cuervo, A. M., and Macian, F. (2010). Macroautophagy regulates energy metabolism during effector t cell activation. *J. Immunol.* 185, 7349–7357. doi: 10.4049/jimmunol.1000576

Itoh, T., Fujita, N., Kanno, E., Yamamoto, A., Yoshimori, T., and Fukuda, M. (2008). Golgi-resident small GTPase Rab33B interacts with Atg16L and modulates autophagosome formation. *Mol. Biol. Cell* 19, 2916–2925. doi: 10.1091/mbc.E07

Jia, W., He, M. X., McLeod, I. X., Guo, J., Ji, D., and He, Y. W. (2015). Autophagy regulates T lymphocyte proliferation through selective degradation of the cell-cycle inhibitor CDKN1B/p27Kip1. *Autophagy* 11, 2335–2345. doi: 10.1080/15548627.2015.1110666

Kabat, A. M., Harrison, O. J., Riffelmacher, T., Moghaddam, A. E., Pearson, C. F., Laing, A., et al. (2016). The autophagy gene Atg16l1 differentially regulates Treg and TH2 cells to control intestinal inflammation. *Elife* 5:e12444. doi: 10.7554/eLife.12444

Karow, M., Fischer, S., Meßling, S., Konertz, R., Riehl, J., Xiong, Q., et al. (2020). Functional characterisation of the autophagy ATG12˜5/16 complex in dictyostelium discoideum. *Cells* 9:1179. doi: 10.3390/cells9051179

Kasai, M., Tanida, I., Ueno, T., Kominami, E., Seki, S., Ikeda, T., et al. (2009). Autophagic compartments gain access to the mhc class ii compartments in thymic epithelium. *J. Immunol.* 183, 7278–7285. doi: 10.4049/jimmunol.0804087

Keady, B. T., Le, Y. Z., and Pazour, G. J. (2011). IFT20 is required for opsin trafficking and photoreceptor outer segment development. *Mol. Biol. Cell* 22, 921–930. doi: 10.1091/mbc.E10-09-0792

Knævelsrud, H., Søreng, K., Raiborg, C., Håberg, K., Rasmuson, F., Brech, A., et al. (2013). Membrane remodeling by the PX-BAR protein SNX18 promotes autophagosome formation. *J. Cell Biol.* 202, 331–349. doi: 10.1083/jcb.201205129

Kovacs, J. R., Li, C., Yang, Q., Li, G., Garcia, I. G., Ju, S., et al. (2012). Autophagy promotes T-cell survival through degradation of proteins of the cell death machinery. *Cell Death Differ.* 19, 144–152. doi: 10.1038/cdd.2011.78

Mason, J. M., and Arndt, K. M. (2004). Coiled coil domains: stability, specificity, and biological implications. *Chembiochem* 5, 170–176. doi: 10.1002/cbic.200300781

Mauthe, M., Orhon, I., Rocchi, C., Zhou, X., Luhr, M., Hijlkema, K. J., et al. (2018). Chloroquine inhibits autophagic flux by decreasing autophagosome-lysosome fusion. *Autophagy* 14, 1435–1455. doi: 10.1080/15548627.2018.1474314

Mizushima, N., Noda, T., Yoshimori, T., Tanaka, Y., Ishii, T., George, M. D., et al. (1998). A protein conjugation system essential for autophagy. *Nature* 395, 395–398. doi: 10.1038/26506

Nedjic, J., Aichinger, M., Emmerich, J., Mizushima, N., and Klein, L. (2008). Autophagy in thymic epithelium shapes the T-cell repertoire and is essential for tolerance. *Nature* 455, 396–400. doi: 10.1038/nature07208

Omori, Y., Zhao, C., Saras, A., Mukhopadhyay, S., Kim, W., Furukawa, T., et al. (2008). Elipsa is an early determinant of ciliogenesis that links the IFT particle to membrane-associated small GTPase Rab8. *Nat. Cell Biol.* 10, 437–444. doi: 10.1038/ncb1706

Otomo, A., Kunita, R., Suzuki-Utsunomiya, K., Ikeda, J. E., and Hadano, S. (2011). Defective relocalization of ALS2/alsin missense mutants to Rac1-induced macropinosomes accounts for loss of their cellular function and leads to disturbed amphisome formation. *FEBS Lett.* 585, 730–736. doi: 10.1016/j.febslet.2011.01.045

Pacini, S., Ulivieri, C., Di Somma, M. M., Isacchi, A., Lanfrancone, L., Pelicci, P. G., et al. (1998). Tyrosine 474 of ZAP-70 is required for association with the Shc adaptor and for T-cell antigen receptor-dependent gene activation. *J. Biol. Chem.* 273, 20487–20493. doi: 10.1074/jbc.273.32.20487

Pampliega, O., Orhon, I., Patel, B., Sridhar, S., Díaz-Carretero, A., Beau, I., et al. (2013). Functional interaction between autophagy and ciliogenesis. *Nature* 502, 194–200. doi: 10.1038/nature12639

Paul, S., Kashyap, A. K., Jia, W., He, Y. W., and Schaefer, B. C. (2012). Selective autophagy of the adaptor protein bcl10 modulates t cell receptor activation of NF-κB. *Immunity* 36, 947–958. doi: 10.1016/j.immuni.2012.04.008

Pazour, G. J., Baker, S. A., Deane, J. A., Cole, D. G., Dickert, B. L., Rosenbaum, J. L., et al. (2002). The intraflagellar transport protein, IFT88, is essential for vertebrate photoreceptor assembly and maintenance. *J. Cell Biol.* 157, 103–113. doi: 10.1083/jcb.200107108

Prevo, B., Scholey, J. M., and Peterman, E. J. G. (2017). Intraflagellar transport: mechanisms of motor action, cooperation, and cargo delivery. *FEBS J.* 284, 2905–2931. doi: 10.1111/febs.14068

Progida, C., Cogli, L., Piro, F., De Luca, A., Bakke, O., and Bucci, C. (2010). Rab7b controls trafficking from endosomes to the TGN. *J. Cell Sci.* 123, 1480–1491. doi: 10.1242/jcs.051474

Pua, H. H., Dzhagalov, I., Chuck, M., Mizushima, N., and He, Y.-W. (2007). A critical role for the autophagy gene Atg5 in T cell survival and proliferation. *J. Exp. Med.* 204, 25–31. doi: 10.1084/jem.20061303

Puleston, D. J., Zhang, H., Powell, T. J., Lipina, E., Sims, S., Panse, I., et al. (2014). Autophagy is a critical regulator of memory CD8+ T cell formation. *Elife* 3, 1–21. doi: 10.7554/eLife.03706

Puri, C., Renna, M., Bento, C. F., Moreau, K., and Rubinsztein, D. C. (2013). Diverse autophagosome membrane sources coalesce in recycling endosomes. *Cell* 154, 1285–1299. doi: 10.1016/j.cell.2013.08.044

Ravikumar, B., Imarisio, S., Sarkar, S., O'Kane, C. J., and Rubinsztein, D. C. (2008). Rab5 modulates aggregation and toxicity of mutant huntingtin through macroautophagy in cell and fly models of Huntington disease. *J. Cell Sci.* 121, 1649–1660. doi: 10.1242/jcs.025726

Ravikumar, B., Moreau, K., Jahreiss, L., Puri, C., and Rubinsztein, D. C. (2010). Plasma membrane contributes to the formation of pre-autophagosomal structures Europe PMC Funders Group. *Nat.Cell Biol.* 12, 747–757. doi: 10.1038/ncb2078

Staiano, L., and Zappa, F. (2019). Hijacking intracellular membranes to feed autophagosomal growth. *FEBS Lett.* 593, 3120–3134. doi: 10.1002/1873-3468.13637

Valdor, R., Mocholi, E., Botbol, Y., Guerrero-Ros, I., Chandra, D., Koga, H., et al. (2014). Chaperone-mediated autophagy regulates T cell responses through targeted degradation of negative regulators of T cell activation. *Nat. Immunol.* 15, 1046–1054. doi: 10.1038/ni.3003

Vivar, O. I., Masi, G., Carpier, J., Magalhaes, J. G., Galgano, D., Pazour, G. J., et al. (2016). IFT20 controls LAT recruitment to the immune synapse and T-cell activation in vivo. *Proc. Natl. Acad. Sci. U.S.A.* 113, 386–391. doi: 10.1073/pnas.1513601113

Wei, J., Long, L., Yang, K., Guy, C., Shrestha, S., Chen, Z., et al. (2016). Autophagy enforces functional integrity of regulatory T cells by coupling environmental cues and metabolic homeostasis. *Nat. Immunol.* 17, 277–285. doi: 10.1038/ni.3365

Xiong, Q., Li, W., Li, P., Yang, M., Wu, C., and Eichinger, L. (2018). The Role of ATG16 in autophagy and the ubiquitin proteasome system. *Cells* 8:2. doi: 10.3390/cells8010002

Xu, X., Araki, K., Li, S., Han, J. H., Ye, L., Tan, W. G., et al. (2014). Autophagy is essential for effector CD8 + T cell survival and memory formation. *Nat. Immunol.* 15, 1152–1161. doi: 10.1038/ni.3025

Zaffagnini, G., and Martens, S. (2016). Mechanisms of selective autophagy. *J. Mol. Biol.* 428, 1714–1724. doi: 10.1016/j.jmb.2016.02.004

Zucchetti, A. E., Bataille, L., Carpier, J. M., Dogniaux, S., San Roman-Jouve, M., Maurin, M., et al. (2019). Tethering of vesicles to the Golgi by GMAP210 controls LAT delivery to the immune synapse. *Nat. Commun.* 10:2864. doi: 10.1038/s41467-019-10891-w

Conflict of Interest: The authors declare that the research was conducted in the absence of any commercial or financial relationships that could be construed as a potential conflict of interest.